

Recent seawater intrusion into deep aquifer determined by the radioactive noble-gas isotopes ^{81}Kr and ^{39}Ar

Yoseph Yechieli^{a,b*}, Reika Yokochi^c, Michael Zilberbrand^d, Zheng-Tian Lu^{e,f}, Roland Purtschert^g, Jürgen Sueltenfuss^h, Wei Jiang^{e,f}, Jake Zappala^{c,e}, Peter Mueller^e, Ryan Bernier^c, Naama Avrahamovⁱ, Eilon Adar^b, Firas Talhami^d, Yakov Livshitz^d, Avihu Burg^a

^aGeological Survey of Israel, 30 Malkei Israel St., Jerusalem 9550161, Israel

^bZuckerberg Institute for Water Research, Ben-Gurion University, Sede Boqer Campus, 8499000, Israel

^cDepartment of the Geophysical Sciences, The University of Chicago, IL, USA

^dHydrological Service, 50 Yirmeyahu St, Jerusalem, Israel

^ePhysics Division, Argonne National Laboratory, Argonne, IL 60439, USA

^fCAS Center for Excellence in Quantum Information and Quantum Physics, Hefei National Laboratory for Physical Sciences at the Microscale, University of Science and Technology of China, Hefei, Anhui 230026, China

^gClimate and Environmental Physics, Physics Institute and the Oeschger Centre for Climate Change Research, University of Bern, Sidlerstrasse 5, 3012 Bern, Switzerland

^hInstitute of Environmental Physics, Section of Oceanography, University of Bremen, Otto Hahn Allee 1, Bremen, 28359, Germany

ⁱEastern R&D Center, Ariel, Science Park, 40700, Israel

Corresponding author:

*(Y. Y.) Phone: 972-2-5314236; fax: 972-2-5380688; email: yechieli@gsi.gov.il

25

26 KEY WORDS

27 Groundwater dating, ^{81}Kr , ^{39}Ar , noble gases, radioactive isotopes, seawater intrusion

28

29 Abstract

30

31 Radioactive noble-gas isotopes tracers ^{81}Kr and ^{39}Ar are used for the first time to measure
32 the residence times of deep (~1000 m) saline coastal groundwater, and to determine its
33 connection mode with the sea. The average rate of seawater intrusion into the deep aquifer in
34 Israel, located near the Mediterranean Sea, is estimated. ^{81}Kr -ages of the saline water samples,
35 found to be younger than 40 ka, contradict previously estimated ages of up to several million
36 years based on hydrogeological considerations. The new results imply a stronger and more recent
37 connection between the aquifer and the sea, and indicate that the intrusion occurred during the
38 sea-level rise that began about 20 ka ago. These coastal aquifers need to be managed with
39 caution because lowering of the adjacent fresh water level due to over pumping could accelerate
40 seawater intrusion in a relatively short time. This study demonstrates the suitability of these two
41 noble-gas tracers for the examination of hydrogeological systems in general and for the study of
42 seawater intrusion in particular.

43

44

45

46

47 **1. Introduction**

48 1.1. General

49 Coastal aquifers are potentially prone to salinization from multiple sources, including
 50 dissolution of subsurface evaporates, ancient trapped seawater, and ongoing seawater intrusion.
 51 The issue of coastal aquifer degradation has become increasingly acute in the past few decades due
 52 to over pumping that induces saline water into adjacent freshwater aquifers. In most cases,
 53 seawater intrusion rates are inferred from increase in salinity (Acworth and Dasey, 2003;
 54 Linderfelt and Turner, 2001), change of chemical composition (Russak et al, 2016; Mercado,
 55 1985), or movement of the fresh-saline water interface (Melloul and Zeitoun, 1999). Direct
 56 determination of the seawater intrusion rate has been done previously, based only on radiocarbon
 57 and tritium tracers (Sivan et al, 2005; Yechieli et al, 2001; Yechieli et al, 2009). However, the
 58 interpretation of radiocarbon results is complicated by water-rock interactions (Mook, 1980), and
 59 dating by tritium becomes ambiguous due to the low values in recent precipitation and its short
 60 half-life. Moreover, saline well water usually mixes with fresh water, further complicating the
 61 chronological interpretation. Noble-gas radionuclides, with chemical inertness, simple source
 62 function, and limited subsurface production, are thus emerging as ideal tracers of groundwater
 63 movement. Indeed, dating of fresh groundwater with noble gases has been performed recently in
 64 many parts of the world, using ^{85}Kr (half life of 10.7 a) and ^3He (decay product of ^3H , whose half
 65 life is 12.4 a) for short-term hydrological processes (Althaus et al, 2009; Visser et al, 2013), ^{39}Ar
 66 (269 a) for intermediate, and ^{81}Kr (229 ka) for long-term processes (Gerber et al, 2017; Aggarwal
 67 et al, 2015). Dating of saline water (even more saline than seawater) was conducted by Sturchio et
 68 al. (2014) but not for the issue of seawater intrusion.

69

70

71 1.2. Site description

72 The Yarkon-Taninim Basin (YTB) of Israel is the western portion of the regional Upper
 73 Cretaceous Mountain aquifer. The basin stretches over 10,500 km², from the water divide in the
 74 Judea and Samaria mountains in the east to the Mediterranean coast in the west (Figure 1). The
 75 northern border of the basin extends to the Yizrael Valley, Mount Carmel, and to the Taninim
 76 spring. The southern border extends into the Sinai Peninsula in Egypt and to the northern Negev
 77 desert (Goldshoff et al, 1980; Shachnai, 1980; Weinberger et al, 1994; Dafny et al, 2010).
 78 Precipitation in most of the YTB drainage basin is about 550 mm/year, all occurring in winter
 79 Mediterranean rain events, and the recharge coefficient is 30-33% (Dafny et al, 2010; Guttman and
 80 Zukerman 1995).

81 The major hydrogeological unit of the YTB is the Judea Group built of 600-900 m thick
 82 Upper Cretaceous karstic limestones and dolomites with some marls and chalks. The aquifer is
 83 divided into upper and lower sub-aquifers by a leaky marly aquitard. The units in the aquifer are
 84 continuous throughout the entire basin and generally dip to the west. In the eastern areas (Judea
 85 and Samaria mountains), the aquifer is exposed and directly replenished by rainfall (Figure 2).
 86 Westwards, the aquifer becomes confined under relatively thick impermeable chalks and marls of
 87 the Senonian Mount Scopus Group and the Eocene Avedat Group. The phreatic parts of the
 88 aquifer, as well as the eastern confined part, contain mostly high-quality young groundwater. A
 89 lateral lithological transition from the karstic permeable Judea Group rocks to the mainly
 90 argillaceous and impermeable Talme Yafe facies (Figure 2) occurs at the western margins of the
 91 basin, mostly along the Mediterranean shoreline (Bein, 1974). This impermeable unit was assumed

to act as a bidirectional hydrological barrier between the Mediterranean Sea and the Judea Group aquifer, preventing flow toward the sea. This results in northward flow of the fresh water within the confined part of the aquifer towards the two natural outlets: the Yarkon springs in the central part of the basin and the Taninim springs at its northern tip (Figure 1). This main and long S-N flow trajectory is fed all along by recharge water that joins the main trajectory from the east (Figure 1).

The northwestern confined portion of the YTB, north of the city of Netanya, contains saline groundwater (Rosenthal et al, 1999) (Figure1). In this area, an unusually sharp (~10m from 20% to 80% seawater) and almost horizontal interface between saline and fresh water is recognized in deep monitoring boreholes (Figure 2). The salinity and chemical composition of this saline water resembles that of the Mediterranean Sea (Cl~22,000 mg/l), while always containing also a small fraction of fresh water of Cl~100 mg/l (at least 10%). Because of the impermeable nature of the Talme Yafe facies, a current hydraulic disconnection to the Mediterranean Sea was assumed, and Neogene trapped seawater (age of several millions years) origin of the salinity in the northwestern part of the aquifer has long been postulated (Rosenthal et al, 1999; Bein and Burg, 2001). In the Neogene, the impermeable clayey Yafo Formation was deposited, which could explain the confinement of this saline water body. However, it should be noted that few hydrological studies suggest current seawater intrusion either directly or along a main fault zone at the northern tip of the basin (Kafri and Arad, 1979; Paster et al, 2006).

In this work, ^{81}Kr and ^{39}Ar tracers are employed for the first time to determine the time scale of the seawater penetration into an adjacent aquifer. These tracers can serve as a diagnostic tool for distinguishing between trapped saline water of Neogene age and active, current seawater intrusion from the Mediterranean Sea. In particular, the results are essential for estimating the

degree of connection between the sea and any nearby active and exploited aquifers, and for minimizing salinization of such coastal aquifers.

2. Materials and Methods

2.1. Field sampling and analytical methods.

Five deep boreholes in the saline part of the western mountain aquifer of YTB (Figure 1) were sampled for chemical analysis of major ions, stable isotopes of oxygen and hydrogen, ^{81}Kr , and other noble gases: two in June 2014 and three in November 2015. Technical details, such as depths of boreholes and intervals of screens, are given in Table 1. Additional samples for ^{39}Ar and ^{14}C analyses were collected in the 2015 campaign. Onsite measurements of pH, dissolved O_2 , water temperature and electrical conductivity were carried out. Two to five cubic meters of groundwater were degassed in the field for radioactive noble gases ^{39}Ar , ^{81}Kr and ^{85}Kr . The field degassing device is based on the hydrophobic membrane contactor. The details about the device and the procedure can be found in Purtschert et al (2013) and Yokochi (2016).

Composition of major ions and stable isotopes were determined according to standard methods in the laboratories at the Geological Survey of Israel, with a maximum error of 3% for chemical parameters (Burg et al., 2006; Russak et al, 2016). The isotopic results of $\delta^{18}\text{O}$ are reported on the SMOW scale and the precision of the measurement is $\pm 0.1\%$. Radiocarbon samples were collected in 200-ml dark sealed glass and measured in the AMS Laboratory, New Zealand. The activities are expressed as a percentage of modern carbon (pMC). The $\delta^{13}\text{C}$ contents were measured in both AMS and GSI Laboratories, and are expressed in permil variations from the Vienna Pee Dee Belemnite Standard (% VPDB). Analyses of ^3H , He isotopes and Ne were conducted at the noble gas laboratory of the Institute of Environmental Physics,

University of Bremen. For the He and Ne analyses, bulk water samples collected in 40-ml copper tubes sealed with pinch-off clamps, were degassed and cryogenically separated by a quadrupole mass spectrometer (Balzers QMG112A) and a high-resolution sector-field mass spectrometer (MAP 215-50). For groundwater samples, the precision of the He and Ne concentrations is better than 1% and for the $^3\text{He}/^4\text{He}$ ratio better than 0.5%. ^3H was analyzed with the ^3He -ingrowth method (Clarke et al, 1976; Sültenfuß et al, 2009) with a precision of $\sim 0.03\text{TU}$: 500 g of water were degassed and stored for the accumulation of the ^3H decay product (^3He) in dedicated He-free glass bulbs. After a storage period of 2-3 months, ^3He was analyzed with a mass spectrometric system.

Separation and purification of krypton and argon from the bulk gas were done in the laboratories of both the University of Chicago and University of Bern using cryogenic absorption and gas chromatography (Purtschert et al, 2013; Yokochi, 2016; Riedmann and Purtschert 2016). The ^{39}Ar activities were measured by low-level gas proportional counting in the Deep Laboratory of the Physics Institute, University of Bern (Loosli, 1983; Loosli et al, 1986; Forster et al, 1992; Riedmann and Purtschert 2016). $^{81}\text{Kr}/\text{Kr}$ and $^{85}\text{Kr}/\text{Kr}$ were measured using the Atom Trap Trace Analysis (ATTA) method (Lu et al, 2013; Jiang et al, 2012; Chen et al, 1999) in the Laboratory for Radiokrypton Dating, Argonne National Laboratory, USA. At least 10 μL STP of Kr gas sample is required for measurement. The ^{81}Kr partial modern values ($R_{81} = (^{81}\text{Kr}/\text{Kr})_{\text{sample}} / (^{81}\text{Kr}/\text{Kr})_{\text{modern}}$) are reported with 1-sigma uncertainty. Partial modern values which exceed the modern atmospheric value defined as due to statistical fluctuations of the ^{81}Kr atom count would represent unphysical groundwater ages of less than zero. The ^{81}Kr apparent age can be calculated with the formula $\text{Age}_{81\text{Kr}} = -t_{1/2}^{81\text{Kr}} \ln(R_{81}) / \ln 2$, where $t_{1/2}^{81\text{Kr}}$ is the half-life of ^{81}Kr . When the sample is young, the measured ^{81}Kr partial modern values could be larger than 1 due to

statistical fluctuations which will result in a negative ^{81}Kr age (younger than modern). In these cases, we adopt the unified method, which is commonly used and well accepted in the high-energy physics community (Feldman and Cousins, 1998). In this approach, we redistribute the groundwater age probabilities into the physical range and obtain ^{81}Kr -age limits with a confidence level of 90%. With this technique, the yielded limit from the measurements will always be physical even when the measurements is not (when $R_{81} > 1$). When the measured data is far from the unphysical region, the errors are simply statistical.

2.2. Relevant processes for data interpretation.

All samples discussed here contain both fresh and saline water components, each with its distinct flow path and residence time. Henceforth, we define age for each component as the time since penetration or recharge of the water into the aquifer. When discussing the saline water, the age (or residence time) is considered to be from the time of penetration of the seawater into the bottom sediment (Yechieli et al, 2009). In such a case, there are three relevant processes: (1) long term seawater intrusion due to natural density-driven circulation near the sea shore; (2) the effect of sea level rise; (3) seawater encroachment landwards due to the short term effect of pumping. The rate of seawater intrusion, and therefore the age of the saline water, would be the result of the superposition of these three possible processes. The initial values of the penetrating seawater can be assumed to be similar to the current ones since the age of the bottom Mediterranean Sea water is probably not more than ~100 years according to their radiocarbon values (Broecker and Gerard, 1969). The age of the fresh water component is determined as the time since recharge into the subsurface, where the water loses its contact with the atmosphere, down to the sampling point.

The interpretation of the ages concluded from two of the noble gases concentrations (^{81}Kr , ^{39}Ar - half-life of 229 ka and 269 years, respectively) is relatively simple since they do not chemically interact with the aquifer's rock and therefore do not require specific corrections for chemical processes (as is the case of ^{14}C , see below). However, physical processes such as diffusive exchange with stagnant water bodies (all tracers, Sanford, 1997) or nucleonic production due to neutron activation of potassium for ^{39}Ar may affect the tracers' concentrations (Lehmann et al, 1993; Purtschert et al, 2004). Practically, diffusion is more pronounced for tracers with longer half-life (e.g. ^{14}C) than for fast decaying tracers. The latter (e.g. ^{39}Ar) do not “see” the total inactive system volume since the time to diffusively reach the inactive volume is much longer than the mean lifetime of the tracer. Therefore, ^{14}C (half-life of 5730 years) is more sensitive to the diffusion process than is ^{39}Ar (half-life of 269 years) resulting in an apparent overestimation of ^{14}C ages compared to ^{39}Ar ages (Mayer et al, 2014). ^{81}Kr ages are similarly affected by this process despite the slightly reduced diffusion coefficient due to the larger mass of the Kr atom. Uncorrected ^{81}Kr ages therefore represent upper age limits if diffusive exchange is ignored.

Moreover, the translation of radiocarbon activities into ages could also be complicated and inconclusive due to chemical processes, such as water-rock interaction and isotopic exchange (Mook, 1980; Gonfiantini and Zuppi, 2013). Thus, dating by ^{14}C is performed with the aid of mass balance equations, using computer codes such as the Netpath and PhreeqC, which take into account the known chemical reactions. These codes estimate one age for any mixed sample (the obtained saline water sample in our case) and do not provide the distinct age of each component in the mixed sample. Since seawater is the larger component in our mixtures, the obtained ages are regarded as a reasonable approximation. An estimated initial value of 60 pMC can be assumed for many cases, also according to the finding in the nearby coastal aquifer,

mainly due to oxidation of old organic matter in the seawater component (Sivan et al, 2005), and due to chemical processes in the unsaturated zone in the fresh water component (e.g. Carmi et al, 2007).

The effect of diffusive exchange between young water in permeable units and old groundwater in less permeable units can increase the apparent radiocarbon age by ~50% in the case of granular aquiferic section separated by clayey impermeable layers and/or when the volume ratio between fractures and rock matrix is relatively low (Sanford, 1997). In the YTB there are indeed less permeable marly units in the karstic carbonate Judea Group aquifer but water and solute can exchange between the karstic channels characterized by very fast water flow and the surrounding porous massive rocks with almost stagnant pore water. The high degree of heterogeneity of the karstic system can lead to a highly dispersive flow and thus wide age distributions (Ghasemizadeh et al, 2012).

219

220 **3. Results and discussion**

The results of all dating tracers are summarized, along with other chemical parameters, in Table 1. The concentration of ^{85}Kr in all gas samples are below the detection limit of ~ 0.5 dpm/ccKr (less than 1% of the current atmospheric concentration of 82 dpm/ccKr). This has two implications: first, contamination of the samples by ambient air during sampling is minimal. Therefore, no correction for air contamination is needed for the ^{81}Kr and ^{39}Ar concentrations. Second, waters are older than ~ 50 years, thus the contribution of young water component is at most relatively small. The very low ^3H concentrations in Raanana Deep (RD) and Taninim 7 (T7) wells (0.01 and 0.05 TU respectively) compared to ~ 3.5 TU in modern precipitation in Israel support the ^{85}Kr data. For Bet Eliezer (BE) well, however, the measured value of ^3H of

0.36 TU is significantly higher, indicating the presence of about 10% young water from the period of 1960-1985, when $^3\text{H}/^{85}\text{Kr}$ ratios in the Earth's surface water were much higher. ^3H - ^3He ages could not be calculated for these three samples since He isotopes and Ne results display large contributions of crustal and mantle helium. Ne concentrations are near equilibrium concentrations of saltwater. In general, crustal He is accumulated in the aquifer with time and therefore is often considered as qualitative age indicator (Sültenfuß 2011 and references therein). Helium concentrations measured in our wells are about two orders of magnitude higher than in air saturated water (ASW 10°C 4.8 10^{-5} cc). Assuming in-situ production only, this corresponds to helium accumulation times in the order of 100kyr. However, the relatively high $^3\text{He}/^4\text{He}$ ratio of $\sim 10^{-6}$ indicates a significant contribution of mantle helium that must enter the aquifer from greater depth. Since external ^4He fluxes can lead to helium accumulation rates 2-3 order of magnitude higher than in-situ production only (Suckow et al., 2013), the measured ^4He concentrations are in accordance with the ^{39}Ar and ^{81}Kr data, which indicate a mixture of water components in the age range of hundreds and 10 thousands of years respectively (see below).

The nearly modern ^{81}Kr activities in all measured samples (Table 1) indicate short water residence time (in terms of ^{81}Kr ages). The lowest value is measured in BE (0.94), indicating an apparent mean residence time of 20 ± 11 ka. The relatively low ^{39}Ar activities ($< 27\%$ mod) implies an age that is older than several hundred years.

All three ^{14}C samples (T7, RD, BE) have low radiocarbon contents (2.9, 3.6 and 5.3 pMC, respectively). Other YTB saline groundwater samples previously analyzed (Burg et al, 2006; Burg and Talhami, 2013) also present low ^{14}C activities, with an inverse correlation between ^{14}C and salinity (Figure 3), suggesting that the fresh water component is much younger than the

saline water. The values of $\delta^{18}\text{O}$ in the more saline samples are close to that of current seawater and plot on a seawater-freshwater mixing line (Figure 4). Accordingly, all samples discussed here are considered as containing different degrees of mixture of seawater and freshwater.

3.1. Residence times of mixed groundwater components.

The saline groundwater in the study area is a mixture of fresh groundwater from the east with proportion (y) and seawater with proportion ($1-y$) that intruded from the west. The mixing proportions are determined by assuming $\text{Cl} \sim 22.5 \text{ g/L}$ and 0 for the seawater (Cl_s) and fresh water (Cl_f) end members respectively according to the following Cl budget:

$$\text{Cl}_m = y \cdot \text{Cl}_f + (1 - y) \cdot \text{Cl}_s$$

where the subscript m refers to the measured chloride concentrations. The resulting fresh water contribution (y) in three samples listed above are in the range of 9-17%. Concentrations of Ar and Kr in the fresh and seawater component are different, and are estimated based on the recharge conditions of both water components: For seawater a recharge elevation of 0 m and salinity of 39‰ and for the freshwater a recharge altitude of 400 meters and a salinity of 0‰ are assumed. No excess air is considered for either water component. Additionally, the solubilities of Ar and Kr are lower in sea water compared to freshwater by a factor of $D=0.82$ (Weiss, 1971; Weiss and Kyser, 1978), , which leads to an adjusted noble gas concentration budget where the contribution of the saline water is reduced by the factor D . The proportion Y of Ar (and Kr) in the freshwater components is then:

$$Y = \frac{y}{y + (1 - y) \cdot D}$$

and $(1-Y)$ for the saline component

$$(1-Y) = \frac{(1-y) \cdot D}{y + (1-y) \cdot D}$$

For ^{39}Ar , the possibility of underground production (Purtschert and Althaus, 2012) also needs to be considered. The lowest measured value of 10% modern at Tananim 7 can be regarded as an upper limit on the secular equilibrium concentration (P) due to underground production. Therefore, an uncertainty range of 0-10% modern is assumed for all samples and for both the sea and the fresh water components. This is justified by the fact that both components were sampled from the same formation, which is built of shallow marine carbonate of relatively uniform composition over a large area.

With the above-calculated mixing proportions of Ar and Kr and the measured concentrations of ^{39}Ar and ^{81}Kr , the following activity budget can be formulated in Eq 1:

$$^{39}\text{Ar}_m = Y_{\text{Ar}} \cdot \left((A_0 - P) \cdot \exp(-\lambda_{\text{Ar}} \cdot t_f) + P \right) + (1 - Y_{\text{Ar}}) \cdot \left((A_0 - P) \cdot \exp(-\lambda_{\text{Ar}} \cdot t_s) + P \right) \quad (1a)$$

$$^{81}\text{Kr}_m = Y_{\text{Kr}} \cdot Kr_0 \cdot \exp(-\lambda_{\text{Kr}} \cdot t_f) + (1 - Y_{\text{Kr}}) \cdot Kr_0 \exp(-\lambda_{\text{Kr}} \cdot t_s) \quad (1b)$$

Underground production is thereby described as an ingrowth process as function of groundwater residence time t , and the secular equilibrium concentration P . Here, the subscript m refers to the measured tracer concentrations, λ 's are the decay constants, and t_f and t_s are the ages of the fresh and saline water components, respectively. A_0 and Kr_0 are initial ratios which equals to present-day atmospheric values. Equations (1a) and (1b) must be fulfilled for any valid pairs of t_f and t_s in consideration of the analytical uncertainties of ^{81}Kr and ^{39}Ar and the possible range of underground production P of ^{39}Ar between 0% modern and 10% modern.

The multi-tracer chronological constraints are depicted in Figure 5 a-c. Each tracer defines an area in the $t_f - t_s$ plane bound by the analytical uncertainties and the uncertainty range of underground production.. The reddish area depicts all possible solutions for ^{39}Ar (Eq 1a) and the grey area for ^{81}Kr (Eq. 2b). For Bet Eliezer, the ^{81}Kr activity can be either mainly originated from the saline water component (in this case the fresh water is over 50 ka old) or from the fresh water component (in this case the saline water is between 13-40 ka). Any intermediate solution between those two extremes is also possible (indicted by the gray band). By adding ^{39}Ar , this range is significantly reduced and only the two shaded areas are left (C1 and C2). Since only C1 is in accordance with the elevated $^3\text{H}/^{85}\text{Kr}$ ratio of Bet Eliezer, indicating the presence of water that recharged close to the peak of the atmospheric bomb tests period (1960-1985), we conclude that the fresh water must be the younger component for this sample, as implied also from the radiocarbon data that indicate an older age for the sea water component (Fig. 3). It can be projected that this is also the case for the other wells,. We therefore add the constraint $t_f < t_s$ for all wells (green line). With these ranges, both the fresh (orange numbers in Fig. 5) and saline (violet numbers) waters are constrained and listed in Table 2. Bet Eliezer is the sample with the youngest fresh water (detectable ^3H) but with the oldest saline water. This is in accordance with the location of the well, which is situated farthest from the coast and thus closest to the current recharge zone in the mountain area

3.2. Implications of radiocarbon signatures.

An activity budget similar to the above Eq (1b) can be formulated for ^{14}C in Eq 2:

$$^{14}C_m = Y_c \cdot C_0 \cdot \exp(-\lambda_c \cdot t_f) + (1 - Y_c) \cdot C_0 \exp(-\lambda_c \cdot t_s) \quad (2)$$

319 The following assumptions are taken into account: (1) an initial activity of 60 pMC; (2) the
 320 above introduced mixing proportion Y_c , using a depletion factor D_c of ~ 0.5 (DIC of saline water
 321 is 50% less compared to freshwater; Burg and Talhami, 2013), and (3) the ages of the fresh and
 322 saline water component deduced above.

323 Accordingly, the calculated ^{14}C activities are 18, 20 and 15 pMC for BE, RD and T7,
 324 respectively. These values are much higher than those measured in the range of 2.9 - 5.3 pMC
 325 (Table 1). Groundwater dating using ^{14}C in the present case, therefore, requires the consideration
 326 of additional processes that reduce the ^{14}C activities in DIC. Meanwhile, the $\delta^{13}\text{C}$ values of the
 327 saline water component are lighter than those of the current seawater, indicating the effect of
 328 oxidation of organic matter of seafloor sediments, containing dead carbon during the seawater
 329 penetration (similar to the process in the shallow coastal aquifer; Sivan et al, 2005). Entering
 330 both the ^{14}C activities and $\delta^{13}\text{C}$ values into PhreeqC or Netpath geochemical codes leads to
 331 adjusted residence time of 21 - 27 ka for the saline water of the YTB (Table S2). The codes
 332 calculated the seawater fractions in the saline groundwater, and the mass transfers (moles) of the
 333 different chemical processes. The main processes are ion exchange (mainly Ca versus Na) and
 334 Ca and Mg dissolution due to dissolution of rock-forming minerals. Another process that might
 335 be of affect is the CO_2 addition due to oxidation of organic matter upon the penetration of the
 336 seawater through the bottom sea sediment and into the aquifer. The apparent difference between
 337 the relatively old apparent radiocarbon ages, and the ages deduced from the ^{39}Ar and ^{81}Kr dating
 338 methods, can be explained by several chemical (water-rock interaction, e.g. Mook, 1980) and
 339 physical (matrix diffusion, Sanford, 1997) processes.

340 Our data can be used to constrain not only the time of seawater intrusion but also the
 341 residence time of the fresh groundwater (constituting 9-17% of the samples). Since HCO_3 in

most fresh water samples is about double than in of seawater, the contribution of carbon from the fresh water could be up to 18-34% of the total. At such mixing ratios, the radiocarbon of the fresh groundwater component has to be 9-30 pMC in the three samples in order to fit the obtained values in these samples which are values of a mixture (Figure 3; Table S1) of fresh and saline water bodies.

Regarding the BE sample, with its relatively high ^{39}Ar and ^3H , there is an unexpected contradiction between the relatively old radiocarbon ages (several thousands of years, 16-30 pMC; Table S1) and the young ^{39}Ar ages (several hundreds of years, >0.27 , Table 1) of the fresh component. Pronounced mixing of the water components with different ages, as expected in a karstic system, is a process that may explain this discrepancy because of the concave exponential decay curve and the shorter half-life of ^{39}Ar compared to ^{14}C . Yet, details of the mixing process cannot be resolved with the restricted available data. It is suggested that the discrepancy could be due to dispersive mixing of several fresh water bodies of different ages and flow rates. The youngest could be the component that percolates into the Samaria Mountains in the east while the oldest could be the water body that moves more slowly at the fresh-saline water interface zone or the component that flows from the farther southern part of the aquifer (Dafny et al, 2010). The mixing of these components is probably due to natural flow near the interface zone.

Loss of ^{14}C from the groundwater into the surrounding aquifer matrix by diffusion is another process that could lead to much older apparent ^{14}C ages (Sanford, 1997). This process would also affect ^{39}Ar and ^{81}Kr but to a different extent as a function of half-life, diffusion coefficients and geometry and spacing of permeable and stagnant zones. This process can explain at least part of the above contradiction in the ages of the BE sample. By assuming similar conditions for the intruding seawater, and similar diffusion with old connate water during the

inland intrusion, the age can be reduced by ~50%. In accordance, the age of the saline water would be younger than that discussed above by ~50% (~10 ka instead of ~20 ka).

3.3. Other age constraints.

More constraints on the age of the saline water can be derived from the isotopic signature. According to the mixing line (Figure 4), the isotopic signature of the old, sea water component is quite similar to that of the present seawater (e.g. $\delta^{18}\text{O}$ of ~1.5‰ and 1.8‰ in old and recent seawater, respectively). Since the isotopic values during most of the period between 15 and 120 ka are different from the present ones by ~1-2‰, it implies that the intrusion took place in sea conditions similar to those of the last 15 ka, or in previous high sea level periods in the Pleistocene (~120 ka ago). Only the former scenario is in accordance with the ^{81}Kr data (Figure 5).

Taking into account all the above age results and analyses, it can be summarized that the intruding seawater is of Holocene age, except the BE sample farther away from the coast showing late Pleistocene age. The intrusion may have been mainly during the last sea level rise or continuous since then.

3.4. Hydrological implication.

The much younger than expected ages of the saline groundwater suggest an active hydraulic connection between the Judea Group aquifer and the Mediterranean Sea. There are two primary hypotheses for the location of this recent penetration (Paster et al, 2006; Dafny, 2009). First is from the northern part of the YTB going southward, either from Or Akiva fault or from the submarine exposure of this aquifer. The second option is through several hydraulic openings

in the impermeable marly Talme Yafe facies, either due to lithological changes or through faults or buried erosional channels filled with coarse-grained sediments with higher permeability. The first hypothesis would result in age gradient from north to south, which was not found in the five ^{81}Kr ages that were obtained in this study. The second hypothesis anticipates increasing seawater residence time with distance from the sea, the indication for this being the oldest age of the BE sample farthest from the coast.

The average rate of seawater intrusion may be estimated from the subsurface residence times. As discussed above, this rate would be superposition of three processes: the natural circulation of seawater in the aquifer, the increased rate due to the rapid rise of sea level in the beginning of the Holocene and effects of over pumping. The effect of sea level rise is expected to be especially significant due to the increase in hydraulic gradient when the sea level rose by 120 m in a relatively short time (Morrissey et al, 2010). Thus, the intrusion of seawater could have occurred over a much shorter time at the transition to the Holocene and could be less active today. However, since the above three processes cannot be separated, the estimation of the rate of intrusion is an average value for the entire distance from the sea to the sampled wells and ignores heterogeneity in this rate. Accordingly, assuming that the flow is from the west to the east and the distance from the contact zone of the aquifer with the sea to the sampled wells is ~20-30 km (Figure 2), and the ages of saline water are about 10 ka, a rough estimation of the average rate of seawater intrusion into the aquifer yields a value of about 2-3 m/year. It is interesting to note that this value is quite similar to a previous estimate in the coastal aquifer of Israel based on geochemical tracers (Sivan et al, 2005), despite the difference in lithology and hydrological conditions. As stated above, this flow rate of saline water could be due partly to

circulation of the seawater below the interface and partly to movement of the whole saline water body inland.

The most important aspect of these results is that the saline water is not Neogenic seawater trapped in isolated pockets in the aquifer. Instead, the young ages and the aging inland imply active, current, hydraulic connectivity between the aquifer and the Mediterranean Sea. Moreover, and from a practical aspect, if the saline water was identified as old, it would have been considered to contain finite volume of storage. The opposite is true if the age is young and the seawater mass in the aquifer is connected to the current sea. In the former case, pumping of the old saline water may be conducted in order to use this water for desalination and decrease the potential risk of increased salinization of the fresh water volume by this problematic water. Such action will have no chance of success in the case of connection with the sea since the water head is permanent and stable (sea level) regardless of the rate of pumping. Consequently, according to our findings over pumping of fresh water in the eastern confined portion of the YTB would draw more saline water from the infinite reservoir of Mediterranean Sea. This important water resource needs to be managed accordingly in order to sustain its quality. Moreover, the fresh-saline water interface may rise in the future in response to the anticipated sea level rise.

4. Summary and conclusions

This work demonstrates that noble gas radionuclides are better than other tracers for determining the rate of seawater intrusion. The multi-tracer approach of these more reliable isotopes provides effective assessments of age structures for both seawater and fresh water components that mixed in the coastal aquifer. Having such new tools will encourage more

similar hydrogeological studies in which new drillings and dating of coastal saline groundwater will enable determination of the connection between the sea and the adjacent aquifer and estimation of the risk of seawater intrusion.

Our results change previous perceptions and indicate that the age of the saline water in the western part of the aquifer is relatively young, and its origin is from active seawater intrusion into the deep confined portion of the aquifer during the Holocene. These young ages imply that pumping of fresh water should be carefully managed due to the risk of salinization by accelerated seawater intrusion, and that the fresh-saline water interface may rise in response to the anticipated sea level rise.

Acknowledgements

Haim Hemo and Iyad Swaed are thanked for their help in field sampling and Roi Ram for helping in data collection and organization. Hana Netzer and Batsheva Cohen (GSI) are thanked for their technical help with the graphics.. The Laboratory for Radiokrypton Dating at Argonne are supported by DOE, Office of Nuclear Physics, under contract DE-AC02-06CH11357. Research seed money for the feasibility study was provided by the University of Chicago and Ben-Gurion University of the Negev. Financial support was also provided by the US–Israel Binational Science Foundation (BSF application 2014351), and by the Israel Water Authority under contract 4501284811. Mekorot Water Company provided access for sampling boreholes and production wells.

456

457 Figure captions

458 Figure 1. Location map of the western Mountain aquifer (Yarkon-Taninim Basin - YTB) and the
 459 sampled wells. Blue arrows denote main directions of fresh groundwater flow. The southern part
 460 of the aquifer (Sinai and northern Negev) is outside the chart. Note the black line which denotes
 461 the western boundary of the YTB Aquifer with the impermeable TalmeYafe group. The green
 462 full circles denote locations of sampled wells, seven of which are given in Table 1 and the rest
 463 taken from previous study of Burg et al. (2006).

464 Figure 2. Schematic cross-section from the Samaria Mountains in the east to the Mediterranean
 465 Sea in the west (see location in Figure 1). Some of the wells are projected onto the cross-section.
 466 The fresh-saline water interface is very close to horizontal. The red broken line denotes possible
 467 seawater intrusion from the sea through openings in the TalmeYafe group.

468 Figure 3. Radiocarbon values versus Cl concentrations, showing the values (blue points) in
 469 groundwater in the studied area as well as the possible values of the fresh and saline end
 470 members. The colored lines are mixing lines according to different values of the initial
 471 concentration (A_0) of the fresh water component. Data are from Table 1 (triangles) and from
 472 previous studies (circles, Burg and Talhami, 2013, Burg et al.,2006).

473 Figure 4. $\delta^{18}\text{O}$ versus Cl concentrations, showing simple mixing line of fresh water with
 474 seawater, implying one source of saline water. Data from Table 1 and from previous studies
 475 (Burg and Talhami, 2013, Burg et al.,2006).

Figure 5. Age ranges of saline and fresh groundwater determined by ^{39}Ar and ^{81}Kr data. The gray areas indicate possible ages based on the ^{81}Kr data and the mixing equation 1b. The bandwidth is defined by the analytical uncertainty as calculated by the unified approach using a 68% confidence limit. The red areas define constraints from the ^{39}Ar data including the analytical uncertainties and a range for underground production between 0-10% modern (Eq 1a). Age ranges that fulfill the constraints for both tracers correspond to the shaded areas. The presence of tritium for Bet Eliezer is only consistent with the assumption that the freshwater component is younger than the saline water (case C1). The criterion $t_f < t_s$ is therefore included for each plot by the green line. The final concluded age bands for the saline (violet numbers) and freshwater (orange numbers) are also given.

490

491 References

- 492 Acworth, R. I.; Dasey, G. R. 2003. Mapping of the hyporheic zone around a tidal creek using a
 493 combination of borehole logging, borehole electrical tomography and cross-creek electrical
 494 imaging, New South Wales, Australia. *Hydrogeology Journal*, 11 (3), 368-377.
- 495 Aggarwal, P. K.; Matsumoto, T.; Sturchio, N. C.; Chang, H. K.; Gastmans, D.; Araguas-
 496 Araguas, L. J.; Jiang, W.; Lu, Z-T.; Mueller, P.; Yokochi, R.; Purtschert, R.; Torgersen, T. 2015.
 497 Continental degassing of 4He by surficial discharge of deep groundwater. *Nature Geoscience*, 8,
 498 35-39.
- 499 Althaus, R.; Klump, S.; Omnis, A.; Purtschert, R.; Kipfer, R.; Stauffer, F.; Kinzelbach, W. 2009.
 500 Noble gas tracers for characterisation of flow dynamics and origin of groundwater: A case study
 501 in Switzerland. *Journal of Hydrology*, 370, 64-72.
- 502 Bein, A. 1974. Reef development at the Judea Group Rocks in the Carmel and in the Israeli coast.
 503 Ph.D Dissertation, The Hebrew University, Jerusalem, Israel, (in Hebrew, English Abstract).
- 504 Bein, A.; Burg, A. 2001. Quantitative, 3-D hydrogeological model for the Yarkon-Tanninim
 505 aquifer as a tool for assessment of operational limitation (“red lines”) and planning of optimal
 506 exploitation, opening report; Rep GSI/28/2001; Geol. Surv. Isr., Jerusalem, Israel, (in Hebrew).
- 507 Broecker, W S; Gerard, R. 1969. Natural radiocarbon in the Mediterranean Sea. *Limnology and*
 508 *Oceanography*, 14 (6), 883-888.
- 509 Burg, A.; Gavrieli, I.; Bein, A.; Fridman V. 2006. *The Yarkon-Taninim aquifer monitoring*
 510 *project; chemical and isotopic compositions in new monitoring wells and other selected wells.*
 511 *Final report*; Rep. GSI/26/2005; (in Hebrew).
- 512 Burg, A.; Talhami, F. 2013. *The Yarkon-Taninim aquifer monitoring project; chemical and*
 513 *isotopic compositions in new monitoring wells and other selected wells, seventh year report.* Rep.
 514 GSI/7/2013. (Geol. Surv. Isr., Jerusalem; (in Hebrew).

- Carmi, I.; Kronfeld, J.; Yechieli, Y.; Yakir, D.; Stiller, M.; Boaretto, E. 2007. Quantitative extraction of dissolved inorganic carbon (as CO₂) and water by vacuum distillation from sediments of the unsaturated zone for carbon isotope analysis (¹³C and ¹⁴C). *Radiocarbon*, 49 (1), 83-94.
- Chen, C. Y.; Li, Y. M.; Bailey, K.; O'Connor, T. P.; Young, L.; Lu, Z-T. 1999. Ultrasensitive isotope trace analyses with a magneto-optical trap. *Science*, 286, 1139.
- Clarke, W. B.; Jenkins, W. J.; Top, Z. 1976. Determination of tritium by mass spectrometric measurement of ³He. *The International Journal of Applied Radiation and Isotopes*, 27, 515-522.
- Dafny, E. 2009. Groundwater Flow and Solute Transport within the Yarkon-Tanninim Aquifer, Israel. Ph.D. Dissertation, Hebrew University, Jerusalem, in Hebrew, English Abstract.
- Dafny, E.; Burg, A.; Gvirtzman, H. 2010. Effects of karst and geological structure on groundwater flow: the case of Yarkon-Tanninim aquifer. Israel. *J. Hydrology*, 389, 260-275.
- Feldman, G.; Cousins, R. D. 1998. Unified approach to the classical statistical analysis of small signals. *Phys. Rev. D.*, 57, 3873.
- Forster, M.; Maier, P.; Loosli, H. H. 1992. Current techniques for measuring the activity of ³⁷Ar and ³⁹Ar in the environment. In *Isotopes of Noble Gases as Tracers in Environmental Studies*; IAEA, Vienna; pp 63–72.
- Gerber, C.; Vaikmäe, R.; Aeschbach, W.; Babre, A.; Jiang, W.; Leuenberger, M.; Lu, Z-T.; Mokrik, R.; Müller, P.; Raidla, V.; Saks, T.; Waber, H. N.; Weissbach, T.; Zappala, J. C.; Purtschert, R. 2017. Using ⁸¹Kr and noble gases to characterize and date groundwater and brines in the Baltic Artesian Basin on the one-million-year timescale. *Geochimica et Cosmochimica Acta*, 205, 187-210.
- Ghasemizadeh, R.; Hellwege, Fr.; Butscher, C.; Padilla, I.; Vesper, D.; Field, M.; Alshawabkeh A. 2012. Review: Groundwater flow and transport modeling of karst aquifers, with particular reference to the North Coast Limestone aquifer system of Puerto Rico. *Hydrogeol J.*, 20 (8), 1441–1461.

- 541 Goldshtoff, Y.; Shachnai, E. 1980. *Yarqon-Taninim-Be'er Sheva basin. Setting and calibrating*
 542 *numerical model*; Rep. 01/80/58; Tahal Ltd., Tel Aviv, Israel; (in Hebrew).
- 543 Gonfiantini, R.; Zuppi, G. M. 2003. Carbon isotope exchange rate of DIC in karst groundwater.
 544 *Chemical Geology*, 197, 319-336.
- 545 Guttman, J.; Zukerman, H. 1995. Yarqon-Taninim – Beer Sheva groundwater basin: setting and
 546 calibrating flow model; Rep. 01/95/72; Tahal Ltd., Tel Aviv, Israel, (in Hebrew).
- 547 Jiang, W.; Bailey, K.; Lu, Z-T.; Mueller, P.; O'Connor, T. P.; Cheng, C-F.; Hu, S-M.; Purtschert,
 548 R.; Sturchio, N. C.; Sun, Y. R.; Williams, W. D.; Yang, G-M. 2012. An atom counter for
 549 measuring ⁸¹Kr and ⁸⁵Kr in environmental samples *Geochimica et Cosmochimica Acta* , 91, 1-6.
- 550 Kafri, U.; Arad, A. 1979. Current subsurface intrusion of Mediterranean seawater – a possible
 551 source of groundwater salinity in the Rift Valley System. *Israel. J. Hydrology* , 44, 267-287.
- 552 Lehmann, B.; Davis, S.; Fabryka, M. J. 1993. Atmospheric and subsurface sources of stable and
 553 radioactive nuclides used for groundwater dating. *Water Resources Research*, 29, 2027-2040.
- 554 Linderfelt, W. R.; Turner, J. V. 2001. Interaction between shallow groundwater, saline surface
 555 water and nutrient discharge in a seasonal estuary: The Swan-Canning System: Special Issue:
 556 Integrating Research and Management for an Urban Estuarine System: The Swan - Canning
 557 Estuary, Western Australia. *Hydrological Processes*, 15 (13), 2631-2653.
- 558 Loosli, H. H. 1983. A dating method with Argon-39. *Earth Planet. Sci. Lett.*, 63, 51-62.
- 559 Loosli, H. H.; Moell, M.; Oeschger, H.; Schotterer, U. 1986. Ten years of low level counting in
 560 the underground laboratory in Bern, Switzerland. *Nuclear Instr. Methods* , B17, 402-405.
- 561 Lu, Z-T.; Schlosser, P.; Smethie Jr., W. M.; Sturchio, N. C.; Fischer, T. P.; Kennedy, B. M.;
 562 Purtschert, R.; Severinghaus, J. P.; Solomon, D. K.; Tanhua, T.; Yokochi, R. 2014. Tracer
 563 Applications of Noble Gas Radionuclides in the Geosciences. *Earth-Science Reviews* , 138, 196-
 564 214.

- Mayer, A.; Sültenfuß, J.; Travi, Y.; Rebeix, R.; Purtschert, R.; Claude, C.; Le Gal La Salle, C.; Miche, H.; Conchetto, E. 2014. A multi-tracer study of groundwater origin and transit-time in the aquifers of the Venice region (Italy). *Appl. Geochem.*, doi:10.1016.
- Melloul, A. J.; Zeitoun, D. G. 1999. A semi-empirical approach to intrusion monitoring in Israeli coastal aquifer. In *Seawater Intrusion in Coastal Aquifers – Concepts, Methods and Practices*; Bear J. et al., Eds.; Kluwer Academic Publishers: The Netherlands; pp 543-558.
- Mercado, A. 1985. The use of hydrogeochemical patterns in carbonate sand and sandstone aquifers to identify intrusion and flushing of saline water. *Ground Water*, 23, 635-645.
- Mook, W. G. 1980. Carbon-14 in hydrogeological studies. In *Handbook of Environmental Isotope Geochemistry, Vol. 1, The Terrestrial Environment*; Fritz, P., Fontes, J. Ch., Eds.; Elsevier Scientific Publishers: New York; pp 49-74.
- Morrissey, S. K.; Clark J. F.; Bennett, M.; Richardson, E.; Stute, M. 2010. Groundwater reorganization in the Floridan aquifer following Holocene sea-level rise. *Nature Geoscience*, 3, 683-687; DOI:10.1038.
- Paster, A.; Dagan, G.; Guttman, J. 2006. The salt-water body in the Northern part of Yarkon-Taninim aquifer: Field data analysis, conceptual model and prediction. *J. Hydrology*, 323, 154-167.
- Purtschert, R.; Loosli, H. H.; Corcho, J. A. 2004. *How reliable are ^{39}Ar ages?*; International Workshop on the Application of Isotope Techniques in Hydrological and Environmental Studies, UNESCO, Paris.
- Purtschert, R.; Althaus, R. 2012. *Ar-39 dating of groundwater: How limiting is underground production?* Goldschmidt Conference; Montreal.

- 588 Purtschert, R.; Sturchio, N. C.; Yokochi, R. 2013. Krypton-81 dating of old groundwater. In
 589 *Isotope methods for dating old groundwater*; eds Suckow, A., Aggarwal, P., Araguas-Araguas,
 590 L., Eds.; IAEA : Vienna; pp 91-124.
- 591 Riedmann, R.; Purtschert, R. 2016. Separation of argon from environmental samples for
 592 Ar-37 and Ar-39 analyses. *Separation and Purification Technology*, 170 DOI:
 593 10.1016/j.seppur.2016.06.017.
- 594 Rosenthal, E.; Weinberger, G.; Kronfeld, J. 1999. Groundwater salinization caused by residual
 595 Neogene and Pliocene sea water: an example from the Judea Group Aquifer, Southern Israel.
 596 *Groundwater*, 37 (2), 261-270.
- 597 Russak, A.; Sivan, O.; Yechieli, Y. 2016. Trace elements (Li, B, Mn and Ba) as sensitive
 598 indicators for salinization and freshening events in coastal aquifers. *Chemical Geology*,
 599 DOI: 10.1016/j.chemgeo.2016.08.003.
- 600 Sanford, W. E. 1997. Correcting for diffusion in carbon-14 dating of groundwater. *Groundwater*,
 601 35, 357-361.
- 602 Shachnai, E. 1980. *Yarqon-Taninim-Be'er Sheva basin, updating the hydrogeological model*;
 603 Rep. 01/80/12; Tahal Ltd., Tel Aviv, Israel, (in Hebrew).
- 604 Sivan, O.; Yechieli, Y.; Herut, B.; Lazar, B. 2005. Geochemical evolution and timescale of
 605 seawater intrusion into the coastal aquifer of Israel. *Geochim Cosmochim Acta*, 69, 579-592.
- 606 Suckow, A. Aggarwal, P.K. and Araguas-Araguas L. 2013. Isotope Methods for Dating Old
 607 Groundwater, IAEA, Vienna, ISBN:978-92-0-137210-9; 357 pp
- 608 Sültenfuß, J.; Rhein, M.; Roether, W. 2009. The Bremen Mass Spectrometric Facility for the
 609 measurement of helium isotopes, neon, and tritium in water. *Isotopes in Environmental and*
 610 *Health Studies*, 45 (2), 1-13.

- Sültenfuß, J., R. Purtschert, J. F. Führböter (2011), Age structure and recharge conditions of a coastal aquifer investigated with ^{39}Ar , ^{14}C , ^3H , He isotopes and Ne. *Hydrogeology Journal*, 19, 221-236.
- Visser, A.; Broers, H. P.; Purtschert, R.; Sültenfuß, J.; de Jonge, M. 2013. Groundwater age distributions at a public drinking water supply well field derived from multiple age tracers (^{85}Kr , $^3\text{H}/^3\text{He}$, and ^{39}Ar). *Water Resources Research*, 49, 7778-7796.
- Weinberger, G.; Rosenthal, E.; Ben-Zvi, A.; Zeitoun, D. G. 1994. The Yarkon-Taninim groundwater basin, Israel hydrogeology: case study and critical review. *J. Hydrology*, 161, 227–255.
- Weiss, R. F. 1971. The effect of salinity on the solubility of argon in seawater. *Deep-Sea Res.*, 18, 225-230.
- Weiss, R. F.; Kyser, T. K. 1978. Solubility of krypton in water and seawater. *J. Chem. Eng. Data*, 23 (1), 69-72.
- Yechieli, Y.; Sivan, O.; Lazar, B.; Vengosh, A.; Ronen, D.; Herut, B. 2001. Radiocarbon in seawater intruding into the Israeli Mediterranean coastal aquifer. *Radiocarbon*, 43, 773-781.
- Yechieli, Y.; Kafri, U.; Sivan, O. 2009. The inter-relationship between coastal sub-aquifers and the Mediterranean Sea, deduced from radioactive isotopes analysis. *Hydrogeol J.*, 17, 265-274.
- Yokochi, R. 2016. Recent developments on field gas extraction and sample preparation methods for radiokrypton dating of groundwater. *Journal of Hydrology*, 540, 368-378.

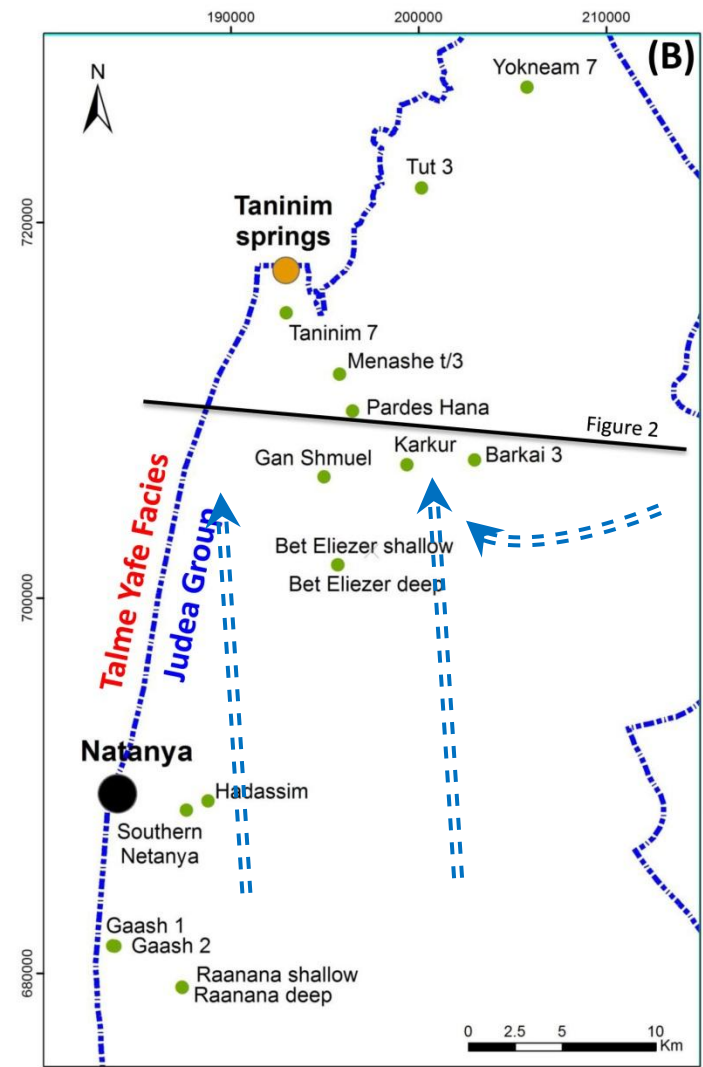
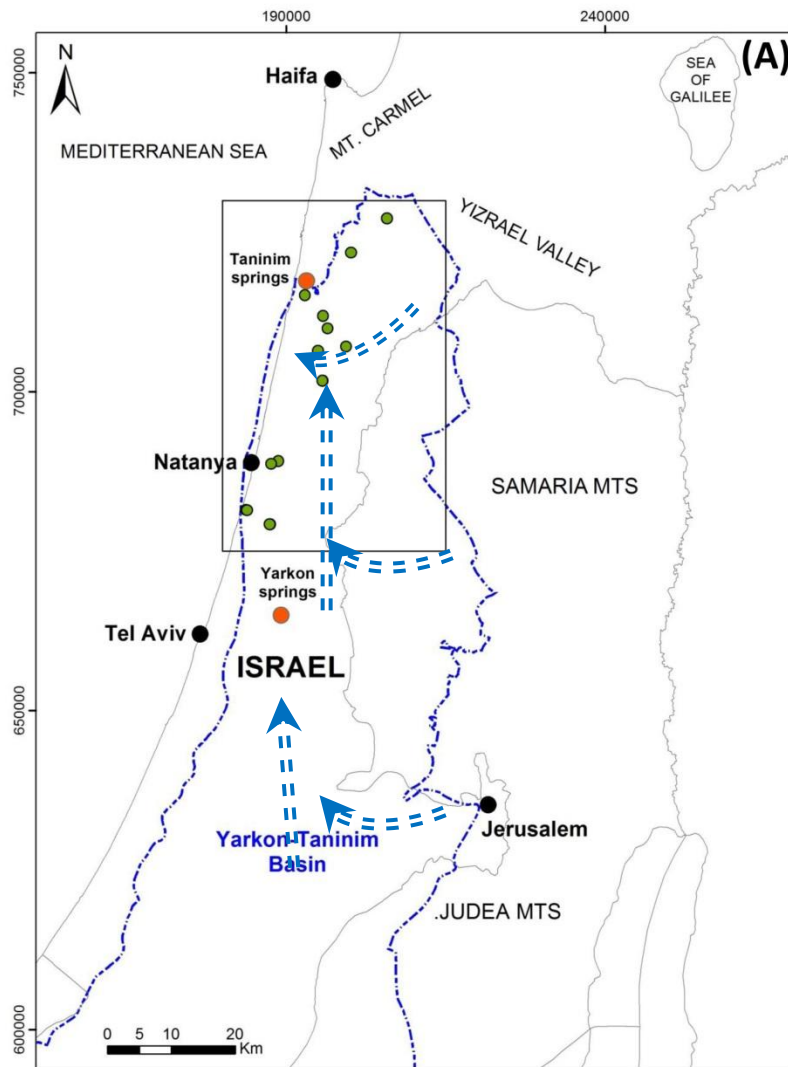


Fig. 1. Location map of the western Mountain aquifer (Yarkon-Taninim Basin - YTB) and the sampled wells. Blue arrows denote main directions of fresh groundwater flow. The southern part of the aquifer (Sinai and northern Negev) is outside the chart. Note the black line which denotes the western boundary of the YTB Aquifer with the impermeable TalmeYafe group.

– WEST –

– EAST –

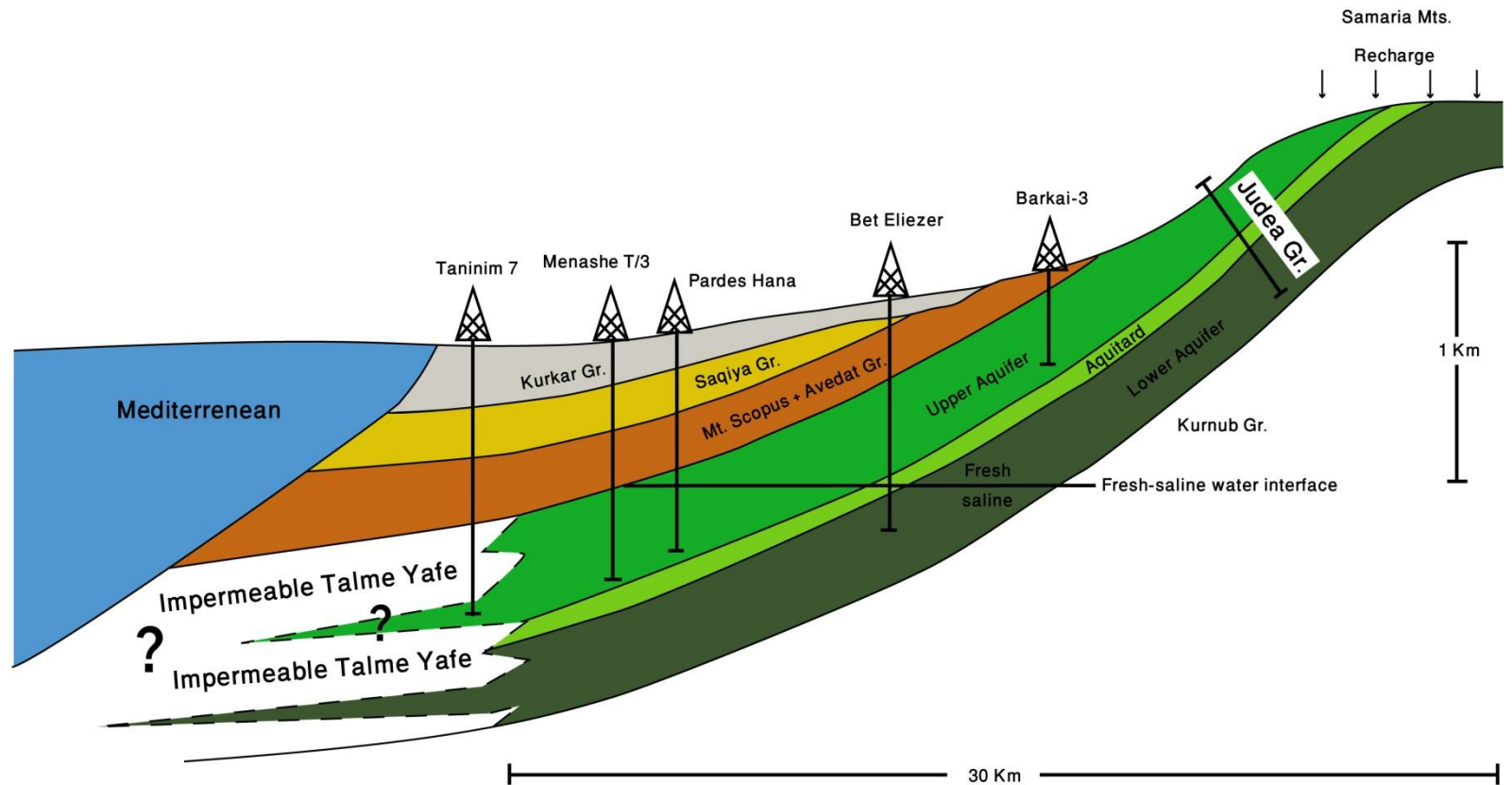


Fig. 2. Schematic cross-section from the Samaria Mountains in the east to the Mediterranean Sea in the west (see location in Figure 1). Some of the wells are projected onto the cross-section. The fresh-saline water interface is very close to be horizontal. The red broken line denotes possible seawater intrusion from the sea through openings in the TalmeYafe group.

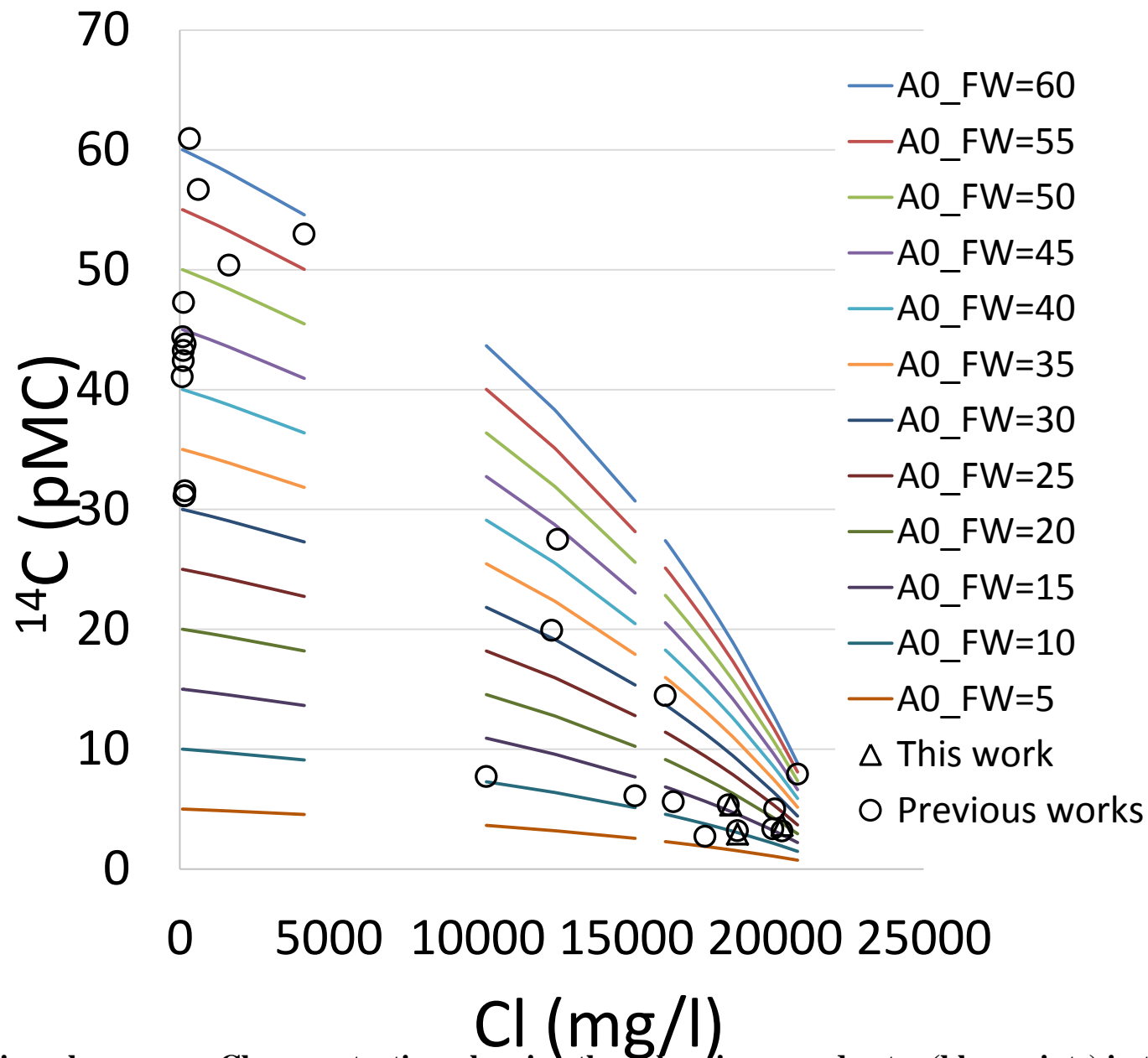


Fig. 3. Radiocarbon versus Cl concentration, showing the values in groundwater (blue points) in the studied area and also the possible values of the fresh and saline end member. The Colored lines are mixing lines according to different values of the initial concentration (A0) of the fresh water component. Data from Table 1 and from Burg et al. (2006) and Burg and Talhami (2013)

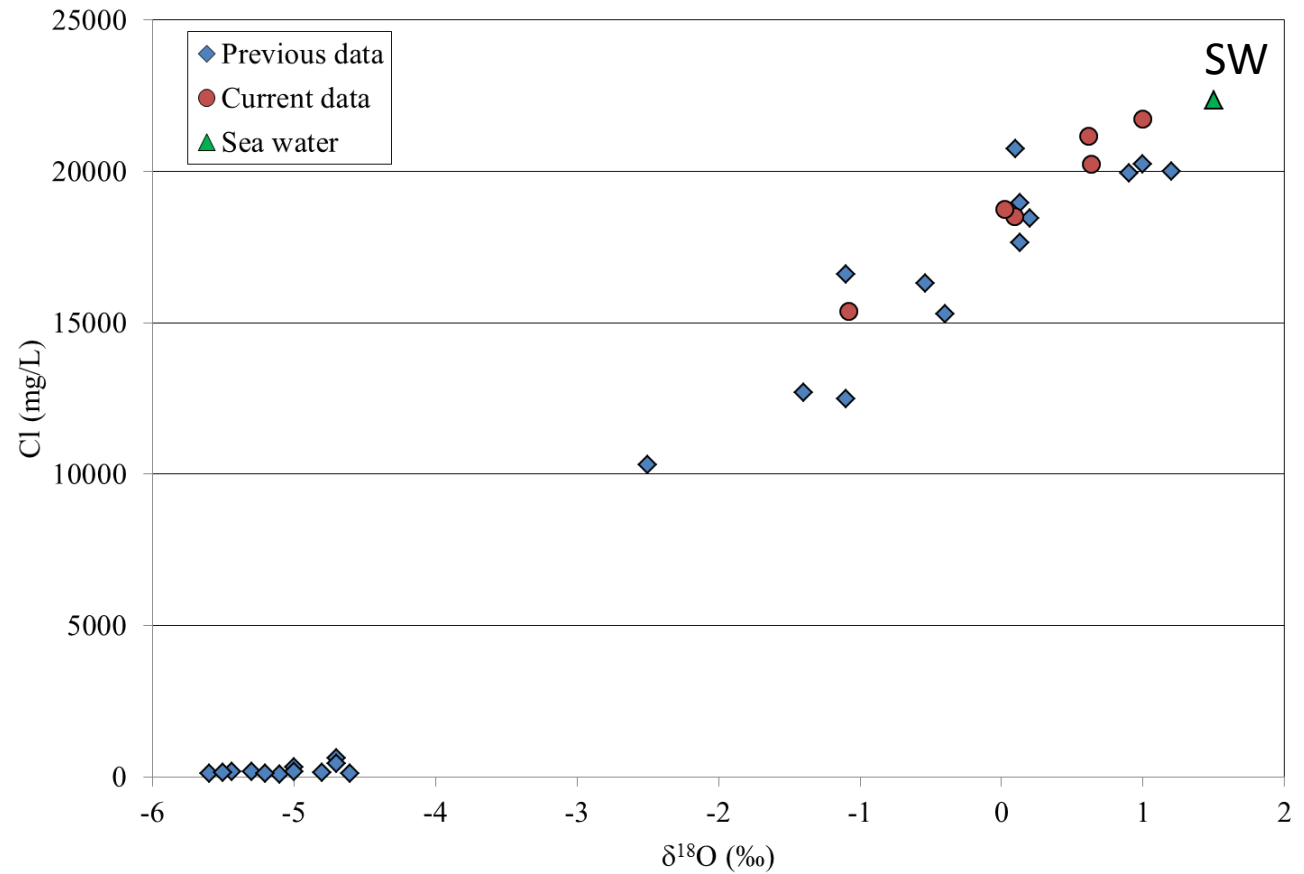


Fig. 4. $\delta^{18}\text{O}$ versus Cl concentrations, showing simple mixing line of fresh water with seawater, implying one source of saline water. Data from Table 1 and from previous studies (Burg and Talhami, 2013, Burg et al., 2006).

Table 1. Technical data and chemical and isotopic analyses

field data and technical details								
name of well	sampling date	EC	DO	filter upper	filter lower	well alltitude masl	temp °c	pH
		millimho	mg/l	m	m			
Menashe T/3	2.6.14	54.2	0	978	1106	19.93	26.9	7.4
Gaash 1	2.6.14	40.5	0	841	1115	31	26.5	7
Gaash 2	2.6.14	53	0	1450	1750	31.02	26.4	7.8
Bet Eliezer deep	15.11.15	40	0	1087	1200	36	27	6.9
Raanana Deep	15.11.15	45	0	1154	1386	53	27	7.1
Taninim 7	15.11.15	45	0	505	645	7.36	27.8	7.2

general chemistry									stable isotopes		
name of well	Na ⁺	K ⁺	Ca ⁺⁺	Mg ⁺⁺	Cl ⁻	SO ₄	HCO ₃ ⁻	TDS #	O-18	H-2	C-13
	mg/L	mg/L	mg/L	mg/L	mg/L	mg/L	mg/L	mg/L	‰	‰	‰
Menashe T/3	12100	525	856	1210	21730	2865	276	39635	0.99	6.7	
Gaash 1	9270	240	358	462	15380	173	386	26327	-1.08	-6.6	
Gaash 2	11320	453	1112	1158	21175	2645	185	38120	0.62	3.0	
Bet Eliezer deep	9453	258	1107	1224	18515	2296	206	33008	0.09	-3.1	-9.6
Raanana Deep	10525	335	1184	1249	20240	2546	192	36228	0.63	-2.7	-6.6
Taninim 7	9169	245	1221	1277	18742	1962	143	32686	0.02	-4.4	-5.9
Medit. seawater	12167	450	441	1482	22371	2928	165	40131	1.5	10	0

noble gases and radiogenic isotopes													
name of well	C-14 water	Ar-39 %	err	⁸⁵ Kr dpm/ccKr	⁸¹ Kr partial modern	err	tritium TU	tritium error TU	³ He ccSTP/kg	⁴ He ccSTP/kg	Ne ccSTP/kg	³ He/ ⁴ He	Ne/He
	pmc	modern											
Menashe T/3				<0.55	1.1	0.05							
Gaash 1													
Gaash 2				<0.4	0.99	0.04							
Bet Eliezer deep	5.32	27	6	<0.69	0.94	0.03	0.36	0.04	5.61E-09	3.66E-03	1.9E-04	1.53E-06	0.05
Raanana Deep	3.62	22	11	<0.5	1	0.03	0.01	0.02	6.43E-09	4.71E-03	1.3E-04	1.37E-06	0.03
Taninim 7	2.91	10	<	<0.66	1.02	0.04	0.05	0.03	5.18E-09	3.64E-03	1.5E-04	1.42E-06	0.04
seawater (in 2015 @ 15°C)	105	100			1		1.00	0.2 estimated	5.12E-12	3.77E-05	1.57E-04	1.36E-06	4.17

Compatibility Report for Table 1 SWI.xls
Run on 1/1/2018 20:20

The following features in this workbook are not supported by earlier versions of Excel. These features may be lost or degraded when opening this workbook in an earlier version of Excel or if you save this workbook in an earlier file format.

Version	# of occurrences	Minor loss of fidelity
Excel 97-2003	1	Some cells or styles in this workbook contain formatting that is not supported by the selected file format. These formats will be converted to the closest format available.

Table 2. Ages of the saline and fresh water components

Sample	Age young fresh (yr)		Age old saline (ka)	
	minimum	maximal	minimum	maximal
Bet Eliezer (BE)	<50	200	13	40
Raanana (RD)	50	1800	0.4	11
Taninim 7 (T7)	900	8000	0.9	8

|
